



3 Wigner Function and Ambiguity Function for Nonparaxial Wavefields

Colin J. R. Sheppard

University of Sydney (Australia)

Kieran G. Larkin

Canon Information Systems Research (Australia)

3.1 Introduction

In the paraxial regime, the Wigner function¹ and ambiguity function² are two phase-space representations that can be used to describe propagation of waves. For example, Brenner, Lohmann, and Ojeda-Castañeda³ described how the ambiguity function can be used as a polar display of the defocused optical transfer function (OTF). However, it is well known that, although these phase-space representations are useful in the paraxial regime, for highly convergent fields their form changes upon propagation, an effect analogous to the introduction of aberrations. Wolf et al.⁴ introduced a form of Wigner function for 2D nonparaxial wavefields called the angle-impact marginal, which has the properties of being real and invariant under translation or rotation.

An alternative representation for wave propagation is based on the concepts of the generalized pupil function, introduced by McCutchen,⁵ and the generalized OTF, introduced by Mertz⁶ and Frieden.⁷ These are 2D or 3D functions for 2D or 3D wavefields, respectively. The term “generalized” is used to distinguish these functions from the ordinary defocused pupil function and OTF, which are defined for a fixed defocus. The generalized transfer functions have been investigated in the paraxial regime, and for highly convergent scalar and vector wavefields.^{8–12} We have found that the concept of the generalized OTF is useful in visualizing the derivation of the Wigner function.¹³

The different representations have also found use in the phase retrieval problem, where knowledge of the intensity in the focal region can be used to reconstruct the phase variations.^{14–18}

3.2 The Ambiguity Function and the 2D OTF for 2D Wavefields in the Paraxial Approximation

The defocused OTF of a convergent wavefield can be expressed directly in terms of the ambiguity function.³ For a convergent quasi-monochromatic wavefield represented by a 1D pupil, the defocused pupil function can be written

$$\begin{aligned} P(m; u) &= P_0(m) \exp(ikW_{20}m^2) \\ &= P_0(m) \exp\left(\frac{1}{2}ium^2\right), \end{aligned} \quad (3.1)$$

where $P_0(m)$ is the in-focus pupil function and m is a normalized spatial frequency so that

$$P_0(m) = 0, \quad |m| > 1. \quad (3.2)$$

Also, W_{20} is the defocus coefficient, $k = 2\pi/\lambda$, and u is a normalized axial displacement

$$u = 4kz \sin^2 \frac{\alpha}{2}, \quad (3.3)$$

where α is the angular aperture of the lens. Defocus is represented by a parabolic phase factor in Eq. (3.1). Then the defocused OTF is given by

$$\begin{aligned} C(m; u) &= \frac{\int P(m' + m/2)P^*(m' - m/2)dm'}{\int |P(m')|^2 dm'} \\ &= \frac{1}{E} \int P_0(m' + m/2)P_0^*(m' - m/2) \exp(iumm') dm', \end{aligned} \quad (3.4)$$

where E is the energy in the beam. All integrals are taken to be evaluated from minus to plus infinity, with the pupil function taken as zero outside of its aperture. The ambiguity function² is defined as

$$A(m, x) = \frac{1}{E} \int P_0(m' + m/2)P_0^*(m' - m/2) \exp(i2\pi m'x) dm'. \quad (3.5)$$

By comparing Eqs. (3.4) and (3.5), we can see a connection between the defocused OTF and the ambiguity function,³ with the relationship

$$um = 2\pi x. \quad (3.6)$$

Papoulis² also considers a function that we call the spectral correlation function, defined as

$$\gamma(m, m') = \frac{1}{E} P_0(m' + m/2)P_0^*(m' - m/2), \quad (3.7)$$

so that we then also have

$$C(m; u) = A\left(m, \frac{um}{2\pi}\right) = \int \gamma(m, m') \exp(iumm') dm'. \quad (3.8)$$

Consider now the 2D generalized pupil function, given by the 1D Fourier transform (in the longitudinal direction) of the defocused pupil function,

$$\Pi(m, s) = P_0(m) \int \exp\left(\frac{1}{2}ium^2\right) \exp(-ius) du. \quad (3.9)$$

The significance of the 2D generalized pupil function is that its 2D inverse Fourier transform gives the amplitude in the focal region. Then there are simple relationships between the 2D generalized pupil function and the 1D in-focus pupil function:

$$\Pi(m, s) = P_0(m) \delta(s - m^2/2), \quad (3.10)$$

and also

$$P_0(m) = \int \Pi(m, s) ds. \quad (3.11)$$

In the same way, the 2D generalized OTF is given by the Fourier transform of the defocused OTF⁶

$$G(m, s) = \int C(m; u) \exp(-ius) du. \quad (3.12)$$

The 2D generalized OTF is given by the autocorrelation of the 2D generalized pupil function. The significance of the 2D generalized OTF is that its 2D inverse Fourier transform gives the intensity in the focal region.

By substituting Eq. (3.8) in Eq. (3.12), we then have

$$G(m, s) = \frac{2\pi}{|m|} \gamma\left(m, \frac{s}{m}\right), \quad (3.13)$$

where

$$s/m = m', \quad (3.14)$$

so that

$$\gamma(m, m') = \frac{|m|}{2\pi} G(m, mm'). \quad (3.15)$$

Equations (3.13) and (3.15) represent a coordinate transformation and a rescaling. In Fig. 3.1 we illustrate how parabolas in m, s space representing contours of

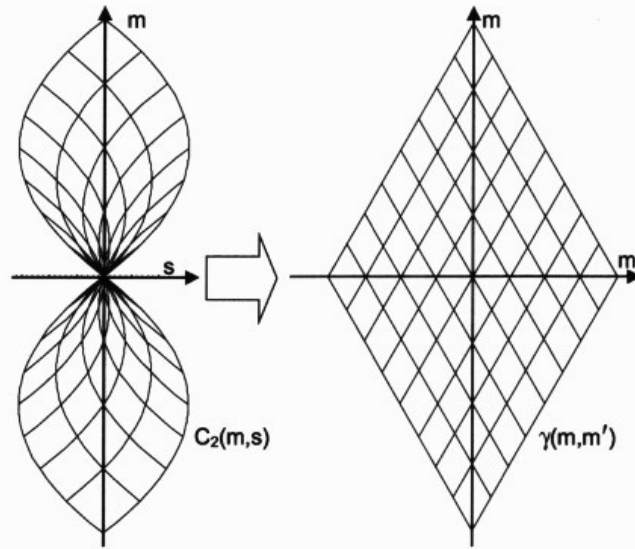


Figure 3.1 The coordinate transformation between the 2D generalized OTF in m, s space and the spectral correlation function in m, m' space. Parabolas in m, s space representing contours of constant $m' \pm m/2$ are mapped into straight lines in m, m' space.

constant $m' \pm m/2$ are mapped into straight lines in m, m' space. Consider as an example an aberration-free pupil of constant amplitude unity for $|m| < 1$. The 2D OTF exhibits a singularity at the origin^{6,7} that is eliminated by the transformation in Eq. (3.15).

In terms of the ambiguity function, inverting Eq. (3.5) leads to

$$G(m, s) = \frac{2\pi}{|m|} \int A(m, x) \exp\left(-\frac{i2\pi xs}{m}\right) dx, \quad (3.16)$$

and inverting Eq. (3.12) results in

$$A(m, x) = \frac{1}{2\pi} \int G(m, s) \exp\left(\frac{i2\pi xs}{m}\right) ds. \quad (3.17)$$

Turning now to the Wigner distribution function¹

$$\begin{aligned} W(m', x') &= \int \gamma(m, m') \exp(i2\pi mx') dm \\ &= \iint A(m, x) \exp[i2\pi(mx' - m'x)] dm dx, \end{aligned} \quad (3.18)$$

we have the relationships

$$G(m, s) = \frac{2\pi}{|m|} \int W\left(\frac{s}{m}, x'\right) \exp(-i2\pi mx') dx' \quad (3.19)$$

and

$$W(m', x') = \int \frac{|m|}{2\pi} G(m, mm') \exp(i2\pi mx') dm. \quad (3.20)$$

In summary, for 2D paraxial wavefields a simple relationship exists between the 2D generalized OTF and the spectral distribution function, representing a coordinate transformation and a rescaling. The defocused OTF is given by a section through the ambiguity function. A Fourier transform relationship exists between the 2D generalized OTF and the ambiguity function.

3.3 The Ambiguity Function and the 3D OTF for 3D Wavefields in the Paraxial Approximation

The treatment of Sect. 3.2 can be extended to the case of 2D pupils. In this case,

$$P(m, n; u) = P_0(m, n) \exp\left[\frac{1}{2}iu(m^2 + n^2)\right], \quad (3.21)$$

the spectral correlation function is

$$\gamma(m, m'; n, n') = \frac{1}{E} P_0(m' + m/2, n' + n/2) P_0^*(m' - m/2, n' - n/2), \quad (3.22)$$

the defocused OTF is

$$C(m, n; u) = \iint \gamma(m, m'; n, n') \exp[iu(mm' + nn')] dm' dn', \quad (3.23)$$

and the ambiguity function is

$$A(m, x; n, y) = \iint \gamma(m, m'; n, n') \exp[i2\pi(m'x + n'y)] dm' dn'. \quad (3.24)$$

In comparing Eqs. (3.23) and (3.24), we have

$$C(m, n; u) = A\left(m, \frac{um}{2\pi}; n, \frac{un}{2\pi}\right). \quad (3.25)$$

Thus, knowledge of the complete defocused OTF determines only a 3D section through the 4D ambiguity function.

The 3D generalized OTF is given by the Fourier transform of $C(m, n; u)$ with respect to u , giving

$$G(m, n, s) = 2\pi \iint \gamma(m, m'; n, n') \delta[s - (mm' + nn')] dm' dn'. \quad (3.26)$$

The 3D generalized OTF is thus given by a line integral on a straight path across the region of overlap of two displaced pupils, as originally pointed out by Frieden.⁷ The 3D generalized OTF can also be expressed in terms of the ambiguity function

$$G(m, n, s) = \int A\left(m, \frac{um}{2\pi}; n, \frac{un}{2\pi}\right) \exp(-ius) du. \quad (3.27)$$

In summary, for 3D paraxial wavefields, knowledge of the complete defocused OTF determines only a 3D section through the 4D ambiguity function. The 3D generalized OTF is given by a line integral on a straight path across the region of overlap of two displaced pupils. The 3D generalized OTF can also be expressed as a Fourier transform of the ambiguity function.

3.4 Derivation of the Angle-impact Wigner Function

For nonparaxial 2D wavefields, the relationship between the 2D generalized OTF and the spectral correlation function is still valid, but the relationship between the ambiguity function and the defocused OTF is no longer simple. The conventionally defined ambiguity function is not a useful representation for high-aperture fields. Therefore, an alternative phase-space treatment called the angle-impact marginal has been introduced.⁴

We consider the 2D problem of a scalar wave propagating in a plane. The amplitude in the focal region can be written as the Fourier transform of the generalized pupil:

$$U(\mathbf{r}) = \frac{k}{2\pi} \iint_{-\infty}^{+\infty} \Pi(\mathbf{m}) \exp(ik\mathbf{m} \cdot \mathbf{r}) d^2\mathbf{m}, \quad (3.28)$$

where $k = 2\pi/\lambda$, and $k\mathbf{m}$ is the wave vector. Because the wavefield satisfies the Helmholtz equation, the generalized pupil is zero except on the surface of the Ewald circle (the 2D form of the Ewald sphere), so that

$$\Pi(\mathbf{m}) = \frac{2\pi}{k} P(\theta) \delta(K - 1), \quad (3.29)$$

where K is the modulus of the vector \mathbf{m} . The intensity in the focal region is

$$I(\mathbf{r}) = \left(\frac{k}{2\pi}\right)^2 \iiint_{-\infty}^{+\infty} \Pi(\mathbf{m}_1) \Pi^*(\mathbf{m}_2) \exp[-ik(\mathbf{m}_2 - \mathbf{m}_1) \cdot \mathbf{r}] d^2\mathbf{m}_1 d^2\mathbf{m}_2. \quad (3.30)$$

Figure 3.2 shows the geometry in spatial frequency space.

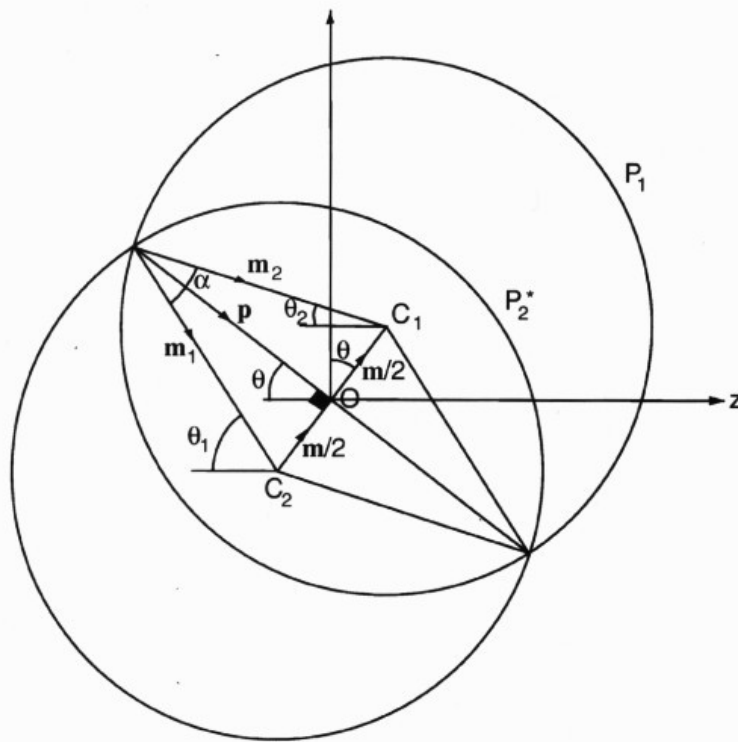


Figure 3.2 Geometry of two intersecting generalized pupil functions. In 2D the pupil functions are circles that intersect in two points. In 3D the pupil functions are spheres that intersect in a circle, with the meridional plane containing the vector \mathbf{m} shown.

If we put

$$\begin{aligned} \mathbf{m} &= \mathbf{m}_1 - \mathbf{m}_2, \\ \mathbf{p} &= \frac{1}{2}(\mathbf{m}_1 + \mathbf{m}_2), \\ K &= |\mathbf{m}|, \end{aligned} \quad (3.31)$$

and

$$p = |\mathbf{p}| = \left(1 - \frac{K^2}{4}\right)^{1/2},$$

then the intensity is

$$I(\mathbf{r}) = \left(\frac{k}{2\pi}\right)^2 \iiint_{-\infty}^{+\infty} \Pi\left(\mathbf{p} + \frac{\mathbf{m}}{2}\right) \Pi^*\left(\mathbf{p} - \frac{\mathbf{m}}{2}\right) \exp(i\mathbf{k}\mathbf{m} \cdot \mathbf{r}) d^2\mathbf{m} d^2\mathbf{p}. \quad (3.32)$$

The intensity can also be written as the Fourier transform of the generalized OTF

$$I(\mathbf{r}) = \frac{k}{2\pi} \iint_{-\infty}^{\infty} G(\mathbf{m}) \exp(i\mathbf{k}\mathbf{m} \cdot \mathbf{r}) d^2\mathbf{m}, \quad (3.33)$$

so that

$$G(\mathbf{m}) = \frac{k}{2\pi} \int_{-\infty}^{\infty} \int_{-\infty}^{\infty} \Pi\left(\mathbf{p} + \frac{\mathbf{m}}{2}\right) \Pi^*\left(\mathbf{p} - \frac{\mathbf{m}}{2}\right) d^2\mathbf{p}, \quad (3.34)$$

i.e., the autocorrelation of the 2D generalized pupil function. In order to calculate this we must take into account the finite spread of frequencies, so that the Ewald circles are in fact rings. Thus the 2D generalized OTF is given by the overlap of two displaced rings, and the overlap depends on the angle of intersection of the rings.^{10,11,18} We then have for \mathbf{m} within the region of support

$$G(\mathbf{m}) = \frac{2\pi P(\theta_1)P^*(\theta_2)}{k |\sin \alpha|}, \quad (3.35)$$

where

$$K = 2 \sin \frac{\alpha}{2}. \quad (3.36)$$

For an unapodized and aberration-free pupil function of semiaperture α , the generalized OTF can be expressed in a simple analytic form. The two rings generally intersect in two points that represent forward- and backward-propagating waves. Thus,

$$I(\mathbf{r}) = \int_{-\infty}^{\infty} \int_{-\infty}^{\infty} \frac{P(\theta_1)P^*(\theta_2)}{|\sin \alpha|} \exp(ik\mathbf{m} \cdot \mathbf{r}) d^2\mathbf{m}. \quad (3.37)$$

We define the spectral correlation function² as

$$\gamma(\alpha, \theta) = P(\theta_1)P^*(\theta_2). \quad (3.38)$$

Note, however, that the arguments in Eq. (3.38) are angles rather than sines of angles as in the Papoulis representation; the pupils are rotated relative to each other. This is a consequence of the geometry of the triangle in Fig. 3.2. The transformation is illustrated in Fig. 3.3. For an optical field of small semiangle, the support (area in which the function is nonzero) repeats periodically. The rectangular region inclined at 45 deg (Fig. 3.4) contains the same information as the square θ_1, θ_2 region, but rearranged. We see that the two points of intersection of the generalized pupils are accounted for by taking both negative and positive values of the variable α .

For the special case of forward-propagating waves only, Eq. (3.35) can be inverted to give

$$\gamma(\alpha, \theta) = \frac{k}{2\pi} |\sin \alpha| G\left(2 \sin \frac{\alpha}{2} \cos \theta, 2 \sin \frac{\alpha}{2} \sin \theta\right). \quad (3.39)$$

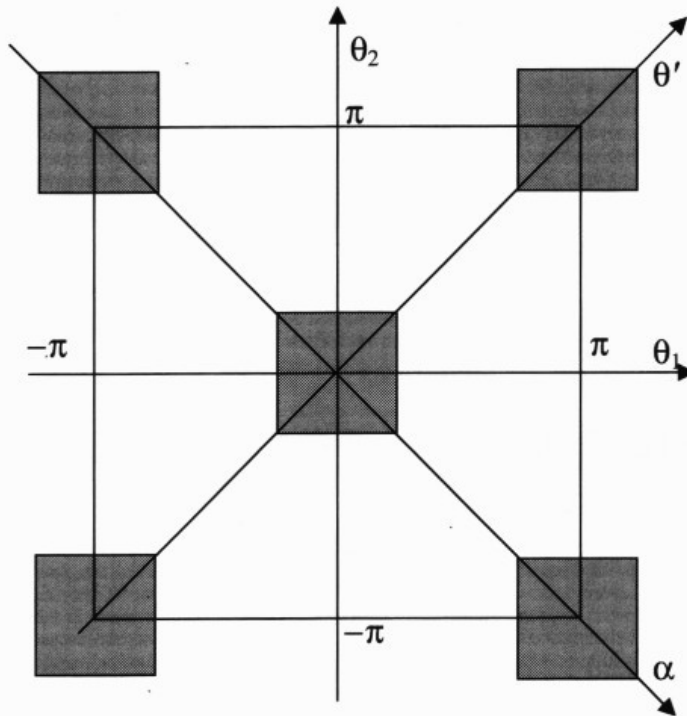


Figure 3.3 The transformation of the integration variables from θ_1, θ_2 to α, θ' . For an optical field of small semiangle, the support (the area in which the function is nonzero) repeats periodically.

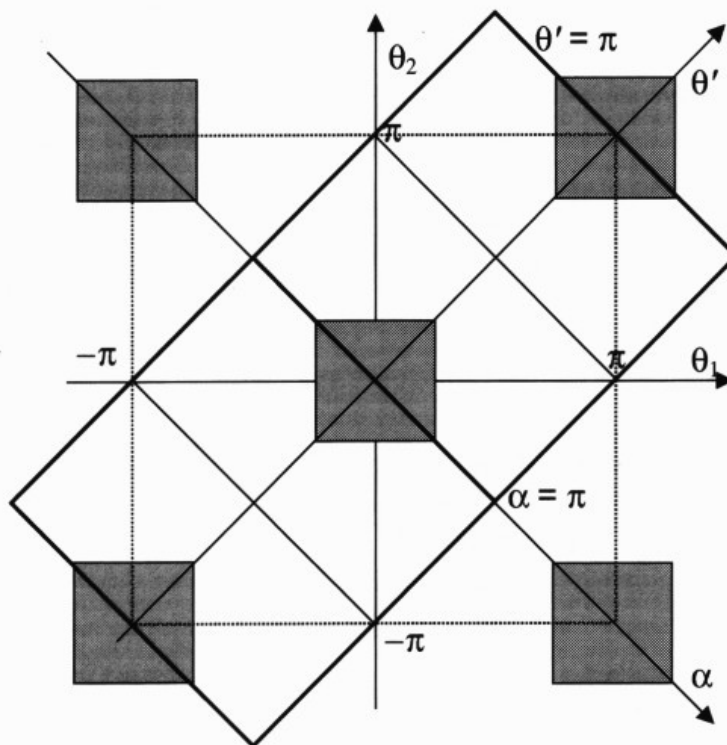


Figure 3.4 The rectangular region inclined at 45 deg contains the same information as the square θ_1, θ_2 region, but rearranged.

We can also introduce the variable

$$m' = \left(1 - \frac{K^2}{4}\right)^{1/2} \sin \theta, \quad (3.40)$$

giving

$$m' = \frac{s}{K} \left(1 - \frac{K^2}{4}\right)^{1/2}, \quad (3.41)$$

which reduces to Eq. (3.14) in the paraxial limit when m' is small.

If we put

$$\ell = \frac{\mathbf{m} \cdot \mathbf{r}}{K} = \hat{\mathbf{m}} \cdot \mathbf{r}, \quad (3.42)$$

transform the integration variables in Eq. (3.37) to coordinates α , θ , and perform the integral in α first, the intensity then becomes

$$I(\mathbf{r}) = \sqrt{\frac{2\pi}{k}} \int_{-\pi}^{\pi} M(\theta, \hat{\mathbf{m}} \cdot \mathbf{r}) d\theta, \quad (3.43)$$

where the angle-impact Wigner function is

$$M(\theta, \ell) = \sqrt{\frac{k}{2\pi}} \int_{-2}^2 \gamma(\alpha, \theta) \frac{\exp(ikK\ell)}{\sqrt{1 - K^2/4}} dK \quad (3.44)$$

$$= \sqrt{\frac{k}{2\pi}} \int_{-\pi}^{\pi} \gamma(\alpha, \theta) \exp\left(2ik\ell \sin \frac{\alpha}{2}\right) d\alpha. \quad (3.45)$$

The geometrical significance of the representation is illustrated in Fig. 3.5. The intensity at any point is expressed over a sum of pairs of plane waves, each of which constitute a ray in the direction \mathbf{p} , at an angle θ to the axis, and with impact parameter ℓ . We note that we have defined ℓ as the scalar product of $\hat{\mathbf{m}}$ and \mathbf{r} , but Wolf et al.⁴ consider it alternatively as a vector product of $\hat{\mathbf{p}}$ and \mathbf{r} .

By inverting Eq. (3.44), we can obtain

$$\gamma(\alpha, \theta) = \sqrt{\frac{k}{2\pi}} \cos \frac{\alpha}{2} \int_{-\infty}^{\infty} M(\theta, \ell) \exp\left(-2ik\ell \sin \frac{\alpha}{2}\right) d\ell, \quad (3.46)$$

which allows the pupil function to be recovered from the Wigner function. We note that for $\ell = 0$, Eq. (3.45) reduces to the circular autocorrelation of the pupil

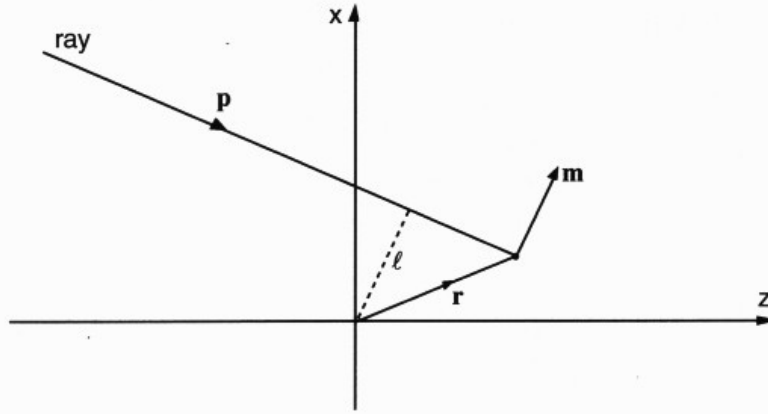


Figure 3.5 The geometrical significance of the angle-impact Wigner function. The intensity at any point is expressed over the sum of pairs of plane waves, each of which constitute a ray in the direction \mathbf{p} , at an angle θ to the axis, and with impact parameter ℓ .

function, but when $\alpha = 0$,

$$|P(\theta)|^2 = \sqrt{\frac{k}{2\pi}} \int_{-\infty}^{\infty} M(\theta, l) dl. \quad (3.47)$$

Alternatively, putting θ_1 or θ_2 constant in Eq. (3.46) allows the angular spectrum to be recovered from the Wigner function to within a constant phase factor. We also have the total energy,

$$\int |P(\theta)|^2 d\theta = \frac{k}{2\pi} \int I(x, z) dl = \sqrt{\frac{k}{2\pi}} \iint M(\theta, l) dl d\theta = E, \quad (3.48)$$

which is a constant invariant under translation or rotation.

For the case of forward-propagating waves only, using Eq. (3.39) we can obtain an explicit Fourier relationship between the generalized OTF and the Wigner function:

$$G(\mathbf{m}) = \sqrt{\frac{2\pi}{k}} \frac{1}{K} \int_{-\infty}^{\infty} M(\theta, l) \exp(-ikKl) dl. \quad (3.49)$$

For a wavefield consisting of both forward- and backward-propagating components, this relationship is generally not possible. The defocused OTF for a forward-propagating wave is given by the 1D Fourier transform of the 2D generalized OTF

$$C(m, z) = \sqrt{\frac{k}{2\pi}} \int G(m, s) \exp(iks z) ds, \quad (3.50)$$

which can be written in the alternative forms

$$C(m, z) = \sqrt{\frac{2\pi}{k}} \int \frac{\gamma(\alpha, \theta)}{\left(\cos^2\theta - \frac{K^2}{4}\right)^{1/2}} \exp(ikKz \tan \theta) d\theta \quad (3.51)$$

$$= \sqrt{\frac{2\pi}{k}} \int \frac{\gamma(\alpha, \theta)}{\left(1 - \frac{K^2}{4}\right)^{1/2} (K^2 - m^2)^{1/2}} \exp\left[ikz(K^2 - m^2)^{1/2}\right] dK. \quad (3.52)$$

For $m = 0$, we then have

$$C(0, z) = \sqrt{\frac{2\pi}{k}} \int_{-\pi}^{\pi} \frac{|P(\theta)|^2}{\cos \theta} d\theta \quad (3.53)$$

for all z , which represents the power flow in the z direction and allows normalization of the OTF.

3.5 Phase Retrieval

Knowledge of the Wigner function allows us to recover the field and the angular spectrum. This is the basis of the phase-retrieval method based on Wigner functions.^{14,15} However, in general, for high-aperture fields, there is an ambiguity caused by the presence of forward- and backward-propagating waves. For example, it is obviously impossible to distinguish, from the intensity in the focal region, whether this was produced by forward- or backward-propagating waves. Thus, the Wigner function also cannot generally be determined from knowledge of the focal intensity.

For the 2D case, when the intensity of a focused field produced by an optical system of semiaperture α is known in the focal region, the modulus and phase of the pupil function (angular spectrum) and the focused field can be recovered by a direct method.¹⁸ The 2D intensity pattern is Fourier transformed to obtain $G(\mathbf{m})$. The coordinates are transformed to give $\tilde{G}(\theta_1, \theta_2)$, which is substituted into Eq. (3.35). Clearly this is a separable function of $P(\theta_1)$ and $P^*(\theta_2)$ that occupies a square region $-\alpha < \theta_1 < \alpha$ and $-\alpha < \theta_2 < \alpha$. Once we have calculated $\tilde{G}(\theta_1, \theta_2)$, we can apply a variety of simple statistical techniques to extract $P(\theta)$, depending on our models of expected noise in the system. Hence, both the phase and modulus (i.e., complex amplitude) of $P(\theta)$ can be found for a coherent field. This requires that we know the wavelength.

In the special case when the wavelength is known and the pupil semiangle is known to be less than π , then there are regions of the spectral correlation function $P(\theta_1)P^*(\theta_2)$ that do not overlap (diagonal regions of $\gamma(\alpha, \theta)$) so that the original phase and amplitude $P(\theta_1)$ can be recovered unambiguously.

Figure 3.6(a) shows an example of an intensity plot for a field that has a semi-angle equal to $\pi/2$. This corresponds to the limiting case when the spectral correlation functions just do not overlap. The spectral correlation function in Fig. 3.6(b) is extracted directly from the intensity map using an algorithm described in detail elsewhere.¹⁸ The magnitude component clearly shows (lighter shade in the grey-scale plot) that the functions do not overlap, but just touch at the corners.

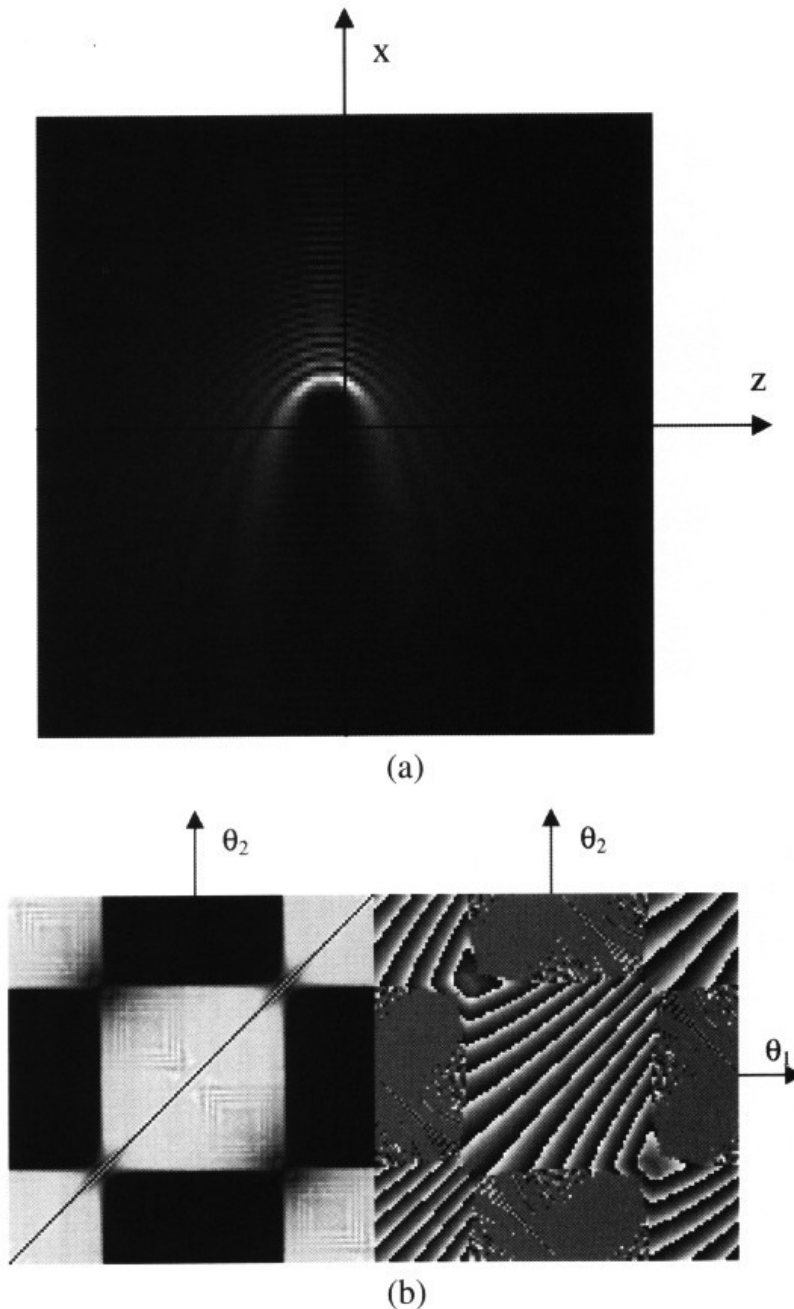


Figure 3.6 (a) An example of an intensity plot for a field with a chirped phase that has a semiangle equal to $\pi/2$. This corresponds to the limiting case for spectral correlation function overlap. (b) The magnitude (left) and phase (right) of the spectral correlation function extracted from the intensity map. The magnitude component clearly shows that the functions do not overlap, but just touch at the corners.

Figure 3.7(a) shows an intensity plot for a field that has a semiangle almost equal to π —in other words, almost the full circle. The spectral correlation function in Fig. 3.7(b) is again extracted from the intensity map. The magnitude component clearly shows almost complete overlap except in an x, y cross pattern at the center. The actual position of the cross depends upon the location of the gap in the propagation direction. The nonoverlapping region allows the phase to be recovered from the intensity information.

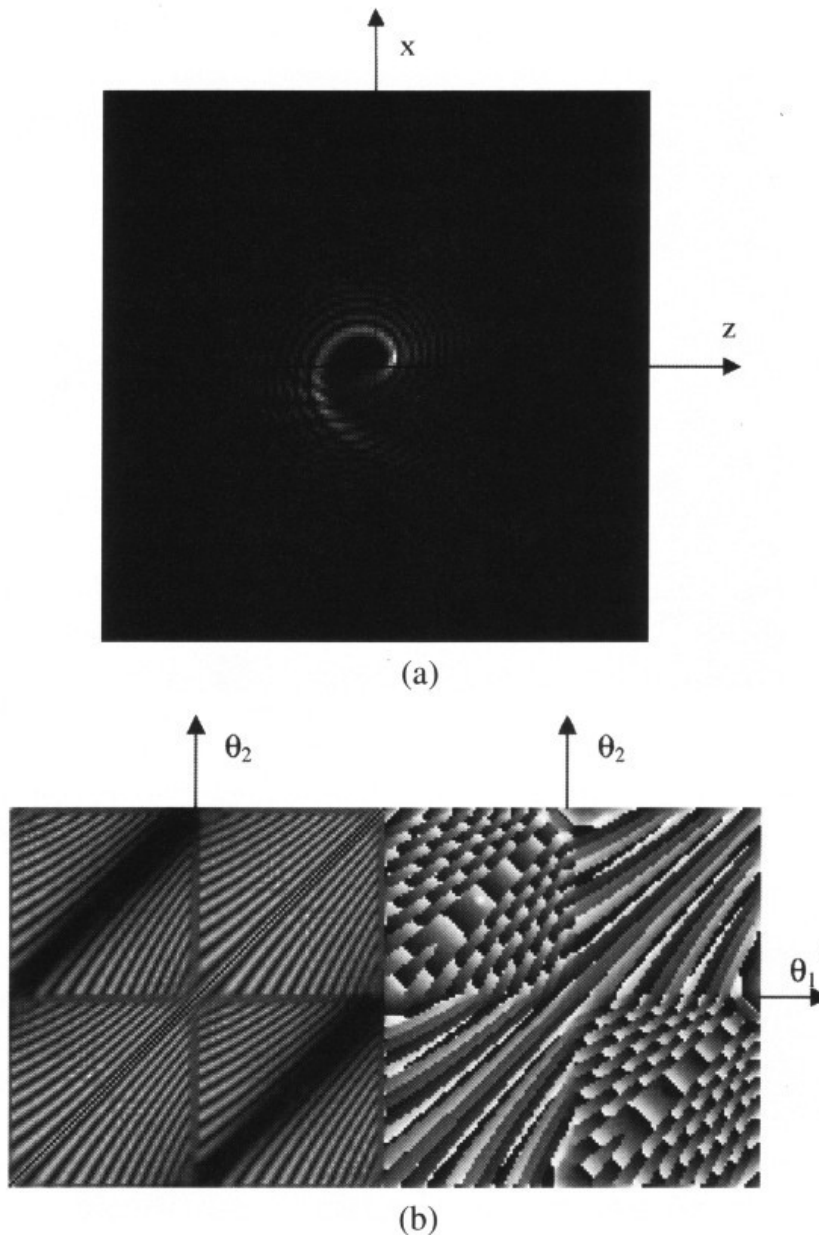


Figure 3.7 (a) An intensity plot for a field with a chirped phase that has a semiangle almost equal to π , in other words almost the full circle. (b) The magnitude (left) and phase (right) of the spectral correlation function again extracted from the intensity map. The magnitude component clearly shows almost complete overlap and interference, except in an x, y cross pattern at the center. The actual position of the cross depends upon the location of the gap in the radiation direction.

3.6 Other Representations

For the paraxial case, the various different functions described are represented in Fig. 3.8. Thus, the generalized OTF $G(m, s)$ is obtained by a 2D Fourier transform of the intensity $I(x, z)$. This 2D Fourier transformation can be performed in two steps in two alternative orders [Fig. 3.8(a)]. If the Fourier transform in x is performed first, we obtain the defocused OTF $C(m, z)$. If, on the other hand, the Fourier transform in z is performed first, we obtain the axial OTF for a displacement x , $D(x, s)$. By the coordinate transformation in Eq. (3.6), the defocused OTF is related to the ambiguity function [Fig. 3.8(b)]. Similarly, the generalized OTF is related to the spectral correlation function through Eq. (3.13). The ambiguity function and Wigner function are also related by a 2D Fourier transformation, and the intensity can be recovered by integration over the Wigner function.

The angle-impact Wigner function can also be regarded as an intermediate step in the transformation between reciprocal space K, θ and real space x, z . Alternatively, the integrals in α and θ in Eqs. (3.43) and (3.45) can be performed in the opposite order. In this case a different intermediate function $B(\mathbf{r}, \alpha)$ is obtained [Fig. 3.9(a)].

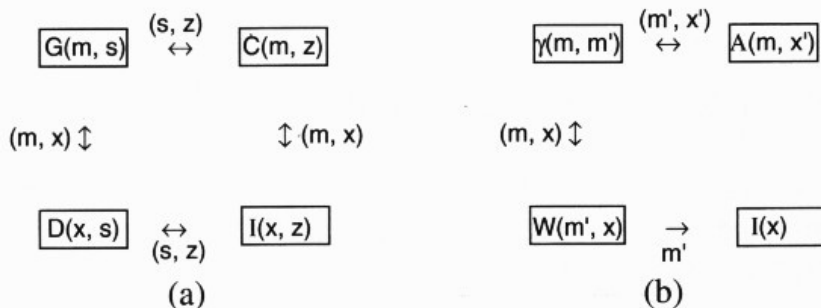


Figure 3.8 The relationship between different representations in the paraxial case, in Cartesian coordinates.

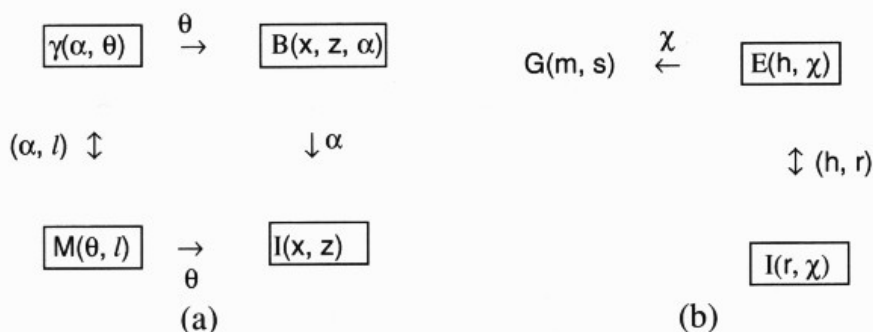


Figure 3.9 The relationship between different representations in the nonparaxial case, in polar coordinates.

We obtain

$$B(\mathbf{r}, \alpha) = \frac{k}{2\pi} \int_{-\pi}^{\pi} \gamma(\alpha, \theta) \exp[ikK(x \cos \theta + z \sin \theta)] d\theta. \quad (3.54)$$

This has the special value

$$B(\mathbf{0}, 0) = \frac{kE}{2\pi}. \quad (3.55)$$

The intensity can be calculated by integrating over K :

$$I(\mathbf{r}) = \frac{2\pi}{k} \int_0^{\infty} \frac{B(\mathbf{r}, \alpha)}{|\sin \alpha|} K dK. \quad (3.56)$$

In the paraxial case, when θ is small and γ is taken as zero outside of its region of support, we then have

$$B(\mathbf{r}, \alpha) = \exp(ikKx) \int_{-\infty}^{\infty} \gamma(\alpha, \theta) \exp(ikKz\theta) d\theta. \quad (3.57)$$

Comparison with Eq. (3.5) shows that $B(\mathbf{r}, \alpha)$ is closely related to the ambiguity function.

In another approach, we start from the intensity rather than the spectral correlation function. In polar coordinates r, χ , once again different intermediate functions are generated [Fig. 9(b)]. By introducing

$$h = \frac{\mathbf{m} \cdot \mathbf{r}}{r} = \mathbf{m} \cdot \hat{\mathbf{r}}, \quad (3.58)$$

we can write

$$G(\mathbf{m}) = \int_{-\pi}^{\pi} E(\chi, \mathbf{m} \cdot \hat{\mathbf{r}}) d\chi, \quad (3.59)$$

where

$$E(h, \chi) = \frac{k}{2\pi} \int_0^{\infty} I(r, \chi) \exp(-ikhr) r dr. \quad (3.60)$$

Then the intensity can be recovered from $E(h, \chi)$:

$$I(\mathbf{r}, \chi) = \frac{k}{2\pi} \int_0^{\infty} E(h, \chi) \exp(ikhr) h dh. \quad (3.61)$$

For forward-propagating wavefields, using Eq. (3.39) we also have for the spectral correlation function

$$\gamma(\alpha, \theta) = \frac{k}{2\pi} |\sin \alpha| \int_{-\pi}^{\pi} E \left[2 \sin \frac{\alpha}{2} \cos(\theta - \chi), \chi \right] d\chi. \quad (3.62)$$

Again, $E(h, \chi)$ has some similarities with the ambiguity function of the paraxial regime.

3.7 Three-Dimensional Wavefields

In the full 3D form of the derivation, the generalized pupil functions are spheres rather than circles, and they intersect in a circle in \mathbf{m} space (Fig. 3.2).¹⁹ We then have

$$I(\mathbf{r}) = \frac{k}{2\pi} \int_{\Omega} \int_0^2 \int_{-\pi}^{\pi} \int_{-\pi}^{\pi} \gamma(\alpha, \theta, \phi, \psi) \exp(-ikml) |m| d\psi d\theta d\phi d^2\Omega, \quad (3.63)$$

where ψ represents the angular position of the point on the intersection circle. If we allow m , and therefore α , to take negative as well as positive values, then we integrate twice over the surface of the sphere, resulting in

$$I(\mathbf{r}) = \frac{k}{4\pi} \int_{\Omega} \int_{-2}^2 \int_{-\pi}^{\pi} \int_{-\pi}^{\pi} \gamma(\alpha, \theta, \phi, \psi) \exp(-ikml) |m| d\psi d\theta d\phi d^2\Omega. \quad (3.64)$$

If we perform the integral in m first, we then have

$$I(\mathbf{r}) = \frac{1}{2} \int_{\Omega} \int_{-\pi}^{\pi} \int_{-\pi}^{\pi} M(\theta, \phi, \hat{\mathbf{m}} \cdot \mathbf{r}, \psi) d\psi d^2\Omega, \quad (3.65)$$

where the angle-impact Wigner function $M(\theta, \phi, \psi)$ is given by

$$M(\theta, \phi, \ell, \psi) = \frac{k}{2\pi} \int_{-2}^2 \gamma(\alpha, \theta, \phi, \psi) \exp(ikK\ell) |K| dK \quad (3.66)$$

$$= \frac{k}{2\pi} \int_{-\pi}^{\pi} \gamma(\alpha, \theta, \phi, \psi) \exp\left(2ik\ell \sin \frac{\alpha}{2}\right) |\sin \alpha| d\alpha. \quad (3.67)$$

The angle-impact Wigner function is related to the 3D generalized OTF by

$$\int_{-\pi}^{\pi} M(\theta, \phi, \ell, \psi) d\psi = \left(\frac{k}{2\pi}\right)^3 \int_{-2}^2 G(\mathbf{m}) \exp(ikK\ell) K^2 dK = N(\theta, \phi, \ell). \quad (3.68)$$

As $G(\mathbf{m})$ is Hermitian, the Wigner function $M(\theta, \phi, \ell, \psi)$ is real. Essentially, this is the reason for integrating twice over the surface of the sphere, as integrating twice allows us to simplify symmetry in all the integration variables. Eq. (3.68) is a Fourier transform if the generalized OTF is taken as zero outside of its passband. It can thus be inverted to give

$$C(\mathbf{m}) = \left(\frac{2\pi}{k}\right)^2 \frac{1}{K^2} \int_{-\infty}^{\infty} M(\theta, \phi, \ell, \psi) \exp(-ikK\ell) d\psi d\ell. \quad (3.69)$$

Eq. (3.66) can also be inverted to give

$$\gamma(\alpha, \theta, \phi, \psi) = \frac{1}{2|\sin(\alpha/2)|} \int_{-\infty}^{\infty} M(\theta, \phi, \ell, \psi) \exp\left(-2ikK\ell \sin \frac{\alpha}{2}\right) d\ell. \quad (3.70)$$

The special case when $\alpha = \pi$ is interesting, as then the integral in ψ in Eq. (3.65) reduces to the evaluation at a single point. We then obtain

$$P(\pi - \theta, \pi - \phi) P^*(\theta, \phi) = \frac{1}{2} \int_{-\infty}^{\infty} M(\theta, \phi, \ell, \psi) \exp(-2ik\ell) d\ell \quad (3.71)$$

for any ψ .

3.8 Discussion

Simple relationships exist in the paraxial regime among the Wigner function, the ambiguity function, the spectral correlation function, and the generalized OTF. It is interesting to note that although the generalized OTF was first introduced in 1965 and phase-space representations have been applied to optics since 1974, the connections between these have not been discussed until recently. Some interesting properties of 3D wavefields were pointed out by Lohmann.²¹

In the nonparaxial regime there is still a simple relationship between the spectral correlation function and the generalized OTF. However, there is no simple relationship, as conventionally defined, with the Wigner function or ambiguity function. The angle-impact Wigner function is related to the spectral correlation function by a Fourier transformation. We can also define functions $B(\mathbf{r}, \alpha)$ and

$E(h, \chi)$, both of which are intermediate functions in polar coordinates between real and reciprocal space that have some similarities with the ambiguity function of the paraxial regime.

Using the spectral correlation function, in the 2D case the phase can be retrieved from knowledge of the intensity even for the nonparaxial case, even if backward-propagating waves are present, as long as there is a known direction for which the pupil function is zero.

Acknowledgments

This chapter is dedicated to the late David Mustard of the University of New South Wales, Australia.

Support is acknowledged from the Australian Research Council and the Science Foundation for Physics within the University of Sydney. This chapter was prepared when C. J. R. Sheppard was Visiting Professor at the Technical University of Delft, The Netherlands.

References

1. M. J. Bastiaans, "The Wigner distribution function applied to optical signals and systems," *Opt. Commun.* Vol. 25, pp. 26–30 (1978).
2. A. Papoulis, "Ambiguity function in Fourier optics," *J. Opt. Soc. Am.* Vol. 64, pp. 779–788 (1974).
3. K.-H. Brenner, A. W. Lohmann, and J. Ojeda-Castañeda, "The ambiguity function as a polar display of the OTF," *Opt. Commun.* Vol. 44, pp. 323–326 (1983).
4. K. B. Wolf, M. A. Alonso, and G. W. Forbes, "Wigner functions for Helmholtz wavefields," *J. Opt. Soc. Am. A* Vol. 16, pp. 2476–2487 (1999).
5. C. W. McCutchen, "Generalized aperture and the three-dimensional diffraction image," *J. Opt. Soc. Am.* Vol. 54, pp. 240–244 (1964).
6. L. Mertz, *Transformations in Optics*, John Wiley and Sons, New York (1965).
7. B. R. Frieden, "Optical transfer of the three-dimensional object," *J. Opt. Soc. Am.* Vol. 57, pp. 56–66 (1967).
8. C. J. R. Sheppard, "The spatial frequency cut-off in three-dimensional imaging," *Optik* Vol. 72, pp. 131–133 (1986).
9. C. J. R. Sheppard, "The spatial frequency cut-off in three dimensional imaging II," *Optik* Vol. 74, pp. 128–129 (1986).
10. C. J. R. Sheppard, T. J. Connolly, and M. Gu, "Scattering by a one-dimensional rough surface and surface reconstruction by confocal imaging," *Phys. Rev. Lett.* Vol. 70, pp. 1409–1412 (1993).
11. C. J. R. Sheppard, M. Gu, Y. Kawata, and S. Kawata, "Three-dimensional transfer functions for high aperture systems obeying the sine condition," *J. Opt. Soc. Am. A* Vol. 11, pp. 593–598 (1994).
12. C. J. R. Sheppard and K. G. Larkin, "Vectorial pupil functions and vectorial transfer functions," *Optik* Vol. 107, pp. 79–87 (1997).

13. C. J. R. Sheppard and K. G. Larkin, "The three dimensional transfer function and phase space mappings," to be published in *Optik*.
14. M. G. Raymer, M. Beck, and D. F. McAlister, "Complex wavefield reconstruction using phase-space tomography," *Phys. Rev. Lett.* Vol. 72, pp. 1137–1144 (1994).
15. D. F. McAlister, M. Beck, L. Clarke, A. Mayer, and M. G. Raymer, "Optical phase retrieval by phase-space tomography and fractional-order Fourier transforms," *Opt. Lett.* Vol. 20, pp. 1181–1183 (1994).
16. J. Tu and S. Tamura, "Wave field determination using tomography of the ambiguity function," *Phys. Rev. E* Vol. 55, pp. 1946–1949 (1997).
17. J. Tu and S. Tamura, "Analytic relation for recovering the mutual intensity by means of intensity information," *J. Opt. Soc. A* Vol. 15, pp. 202–205 (1998).
18. K. G. Larkin and C. J. R. Sheppard, "Direct method for phase retrieval from the intensity of cylindrical wavefronts," *J. Opt. Soc. Am. A* Vol. 16, pp. 1838–1844 (1999).
19. C. J. R. Sheppard and K. G. Larkin, "The Wigner function for highly convergent three-dimensional wavefields," *Opt. Lett.* Vol. 26, pp. 968–970 (2001).
20. C. J. R. Sheppard and K. G. Larkin, "Wigner function for non-paraxial wavefields," to be published in *J. Opt. Soc. Am. A*.
21. A. H. Lohmann, "Three-dimensional properties of wavefields," *Optik* Vol. 51, pp. 105–117 (1978).